A Design of Single-Switch Two-Stage DC-DC Converters With PWM And PFM for Off-Grid Solar Power System

Junkai Zhao, Herbert H.C. Iu, Tyrone Fernando*

(School of Electrical, Electronic and Computer Engineering, The University of Western Australia, 35 Stirling Highway, Crawley, WA 6009, Australia)

Abstract: In this paper, a single-switch two-stage DC-DC conversion circuit is proposed for an off-grid solar power application. A photovoltaic(PV) panel powers the load and a storage unit(battery) via the proposed circuit. The battery is designed to balance the supply and the demand of power under different irradiation situations. Based on conventional cascaded DC-DC converters, the proposed design is developed with the single switch technique reducing size, cost and power loss. The control scheme in this design is pulse width modulation(PWM) with pulse frequency modulation(PFM). The PWM module is similar to conventional design except its ramp signal with a variable frequency is provided by a resettable integrator. As a result, the PWM and PFM modules regulate the two stages of the proposed circuit separately with the same switching control signal. In this paper, the modes of operation of the circuit are discussed as well as the control schemes. The design process is described along with the circuit analysis and comparisons with conventional design are made as well. A prototype has been built to verify the proposed circuit with simulation and experimental results.

Keywords: Single-switch technique, photovoltaic power system, off-grid solar system, DC-DC conversion, resettable integrator, pulse frequency modulation(PWM), pulse width modulation(PFM).

1 Introduction

Renewable energy provides greater options addressing society concerns about the depletion of the fossil fuel. One source of renewable energy, solar energy, is converted from sunlight using Photovoltaic (PV) panels. The solar panels are widely installed for civil use. The power supplied by the solar panels is usually DC and not stable at all times. Therefore DC-DC or DC-AC conversion is required before the solar panels supply the load or are connected to the power grid[1]. Energy storage is also needed to absorb the excess power from the source and supply the load during irradiaton times[2]. The three-port topologies for the renewable energy have been designed and investigated widely by power engineers and researchers. A great number of topologies have been developed for cascaded converters[3] as well as converters working in parallel[4-5]. These converters are built for different circumstances, such as on grid or off-grid applications. The conventional designs normally regulate the converters separately and require a certain number of components, such as at least one switch in each converter. Some studies attempt to combine the components of different converters to improve the circuitry as well as their size and performance[6-8]. In particular, the switch can be shared by the converters with the single switching technique[9-13]. Based on this technique, a design of single switch cascaded converters is developed for an off-grid PV power system. Since the switch has to control two different converters, the Pulse Frequency Modulation (PFM)[14] is introduced to the proposed circuit along with the pulse width modulation (PWM) as the traditional design. The proposed PFM module is developed with a resettable integrator which generates ramp signal with variable frequency. Then the switch control for two converters is achieved simultaneously. The advantages of the proposed circuit include reducing the number of the components as well as the power loss in the power conversion.

This paper consists of the following parts: section 2 introduces the main circuit of the proposed two-stage conversion circuit along with its regulation schemes, its operation modes and the battery modes. Section 3 describes the design process of this study as well as the circuit specifications. The comparison between the proposed design with the conventional is discussed regarding the maximum ratings in this section. The simulation confirms the operation of the proposed circuit along with the experimental results in Section 4. The improvement of the proposed design is given addresing concerns of component cost and switching loss in this section. In the end, Section 5 gives the conclusion of this paper.

2 Proposed circuit

2.1 Main circuit

For the off-grid solar application, a two-stage conversion is applied to deliver power from the input to the load as well as the energy storage unit. A boost converter is series connected to a buck converter in the conventional design shown in Fig.1(a). The battery in the middle of the circuit can store the excess power from the first stage. It supplies the load when there is

* Corresponding Author, E-mail: yis@et.aau.dk.

insufficient or even no input power. The inductors L_1 and L_2 maintain the continuous inductor currents while the capacitors C_1 and C_2 stabilise the battery voltage and the output voltage respectively. For the control simplicity, the two switches S_1 and S_2 are regulated by two independent PWM signals. In other words, the two duty ratios D_1 and D_2 are related to the voltages of their own stages only and different from each other. Meanwhile, the same switching frequency f is applied to both switches unless there is another requirement.

The single switch technique provides the possibility of simplification of the conventional design. In the proposed circuit, the passive components including the two inductors and the two capacitors stay in the same position as well as the diodes D_1 and D_2, as shown in Fig.1(b). However, the two switches of the traditional circuit are replaced with a single S_1 located in the bottom branch with two auxiliary diodes D_3 and D_4 which prevent reverse currents. Since the two stages share the single switch, a unique control signal is required for the correct conversion in both stages.

2.2 Control schemes

Based on the requirements of the proposed application, the control circuit should be able to regulate the voltage of the PV unit according to a reference given by the circuit designer or the maximal power point tracking (MPPT). At the same time, it sustains a constant load voltage.

For conventional converters, two simple PWM controllers generate two pulse signals with different duty ratios D_1 and D_2 for the two switches S_1 and S_2 regulating the PV voltage and the load voltage respectively. The switching frequency f is not specified since it is not relevant to the voltage relationships.

For the proposed design, only one control signal is available for the single switch. In this case, the operational modes of the converters are modified to suit the same switching method in the different stages. To achieve this, the converter in the first stage works under the discontinuous conduction modulation (DCM) with a discontinuous inductor current. Meanwhile, the operation of the battery-load conversion is discontinuous conduction modulation (CCM), the same as the conventional operation. As a result, the control variables of the system become the duty ratio D and the switching frequency f. The load voltage is determined by D only due to CCM. In the first stage, the voltage conversion is related to both the duty ratio D and the switching frequency f as a result of DCM. However, the duty ratio D is governed by the CCM controller and is relatively constant. Thus the frequency f can be treated as the only control variable for the first stage.

The control scheme of the PWM controller is similar to the conventional one for CCM operation, as shown in Fig.2(a). The controller compares the load voltage V_o with the reference V_{o_ref} and generates an error V_{e_pwm}. In the proposed design, this error signal V_{e_pwm} is not compared with a constant ramp signal provided by an oscillator as with the traditional PWM controller. Instead, the ramp waveform is given by the PFM controller. The comparator generates a pulse wave V_{con} determined by the relation of the error and the ramp for the driver to drive the single switch.

The PFM controller provides a sawtooth wave with a relatively fixed magnitude and variable frequency f determined by the PV voltage error V_{e_pfm} as displayed in Fig.2(b). In the PFM controller, the voltage of the solar panel V_{in} is examined based on the reference V_{in_ref}. The error V_{e_pfm} forms the input of a resettable integrator. Since the V_{in} is relatively constant in one period of switching, the input of the integrator is assumed to be constant. Therefore the output of the integrator is a ramp wave with a slope determined by the input. Once the integral is greater than a certain value V_{ramp_ref}, the capacitor of the integrator is shorted and the integrator is reset. With different values of the error V_{e_pfm}, the slope of the ramp is changed so that the width of the ramp is controlled as well as the frequency. In the PFM controller, the V_{ramp_ad} is designed to adjust the input of the integrator. Moreover, PI units are utilized in the proposed design as well as inverters. The schematic diagrams of the PFM control module are given in Fig.3. The control modules are designed with the op-amps for the prototype. Regulation chips with adjustable oscillators can be used to simplify the control modules.

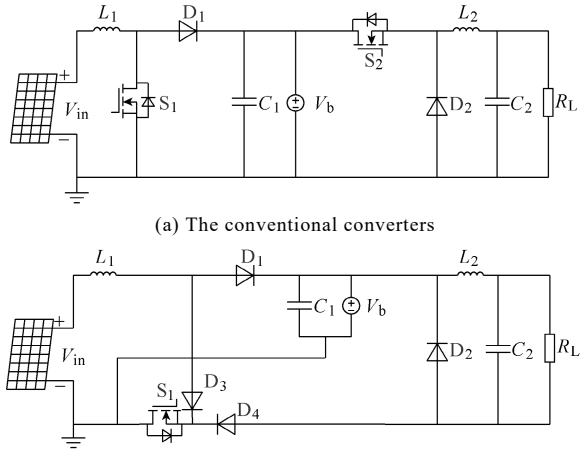

Fig.1 Diagram of cascaded DC-DC converters for the proposed application

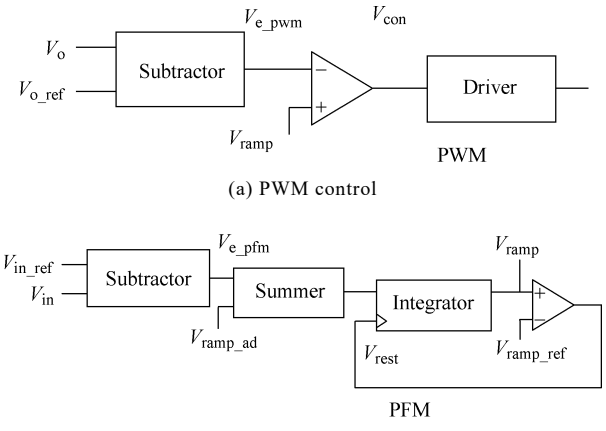

Fig.2 The regulation schemes in the different stages of the proposed circuit

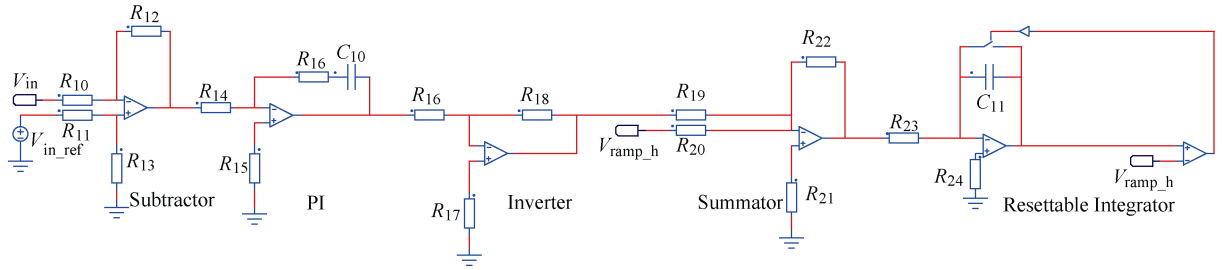

Fig.3 The schematic diagram of the PFM control module

2.3 Operational modes

Three assumptions are given to simplify the circuit analysis of three modes of operation. The first one is that the ideal models are used in the derivation for all components. The second one is the state of charge (SOC) of the battery. Since the function of the storage unit is to balance the input and the output, the battery must be able to be charged or discharged at all times. Lastly, the voltages and currents of both ends of the proposed circuit are constants with neglegable ripples during the whole working period.

The proposed circuit operates in three modes during a switching period. When the single switch is energized, both of the inductors are charged with increasing inductor currents. During the off-time of the switch, the inductor current i_{L2} drops to zero (DCM) while i_{L1} does not (CCM). Therefore the three operational modes are found, as shown in Fig.4.

Mode 1: When the single switch S_1 is conducted, the diode D_3 is forward biased. In this case, the current path is formed by the PV panel (with the input voltage V_{in}), the inductor L_1, the battery, the diode D_3 and the switch S_1 in the first stage, as shown in Fig.4(a). Thus the inductor L_1 is charged by the current i_{L1} with the following slope:

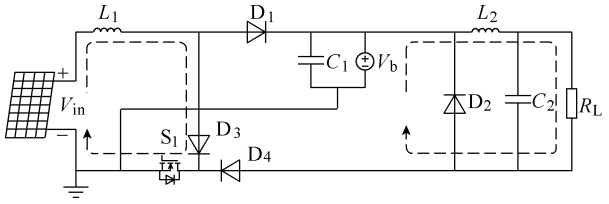

(a) Mode 1

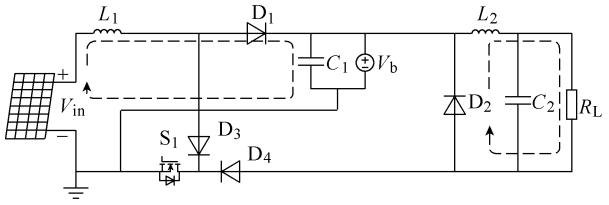

(b) Mode 2

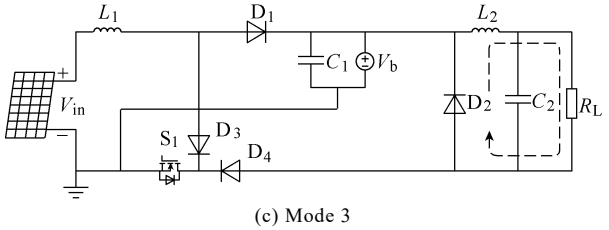

(c) Mode 3

Fig.4 Operational mode of the proposed circuit

$$\frac{di_{L1}}{dt} = \frac{V_{in}}{L_1} \tag{1}$$

Meanwhile, the inductor current i_{L2} is increased due to a charging route which consists of the storage unit (V_b), the inductor L_2, the load (V_o), the diode D_4 and the switch S_1 in the second stage. The slope of the inductor current i_{L2} is given by:

$$\frac{di_{L2}}{dt} = \frac{V_b - V_o}{L_2} \tag{2}$$

Mode 2: After the on-period, the MOSFET S_1 is turned off by the control signal and the proposed circuit operates in mode 2. Both of the inductors start releasing their energy. The current paths are shown in the Fig.4(b). The inductor current i_{L1} flows through the diode D_1 to supply the battery in the first stage. The slope of the inductor current i_{L1} can be found as:

$$\frac{di_{L1}}{dt} = \frac{V_{in} - V_b}{L_1} \tag{3}$$

Similarly, the load loses the power supply from the battery due to the open switch. The current path consists of the inductor L_2, the load and the diode D_2. The inductor current i_{L2} becomes:

$$\frac{di_{L2}}{dt} = \frac{-V_o}{L_2} \tag{4}$$

Mode 3: Once the inductor L_1 is discharged completely, the proposed circuit starts running in this mode. The single switch remains de-energized as in the previous mode. There is no current (i_{L1} =0) flowing in the first stage due to DCM. In contrast, the current i_{L2} has the same discharge slope given by (4) because of CCM.

2.4 Operational modes of the battery

The energy store unit in the proposed converters is designed to provide a stable voltage to the load in different situations. Since the power given by the PV panel does not always match the demand of the load due to some influences like shading, the battery stores the excess power from the input or works as a complementary power supply. Assuming the SOC of the battery is in a range that it can absorb and supply energy, the five operational modes are given in Fig.5 for the battery.

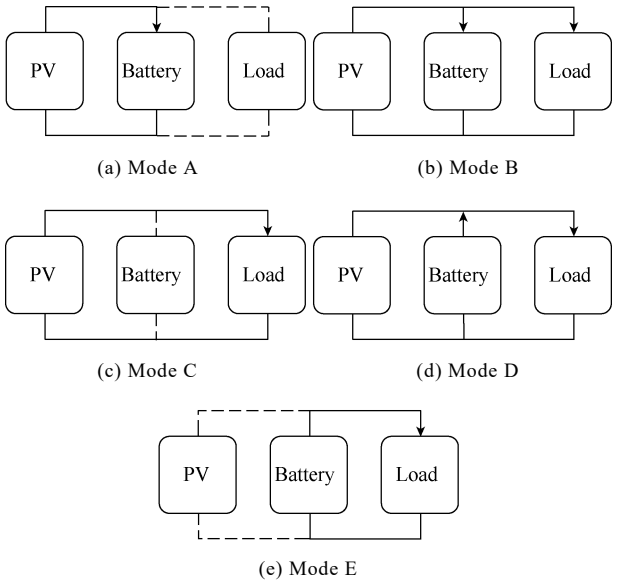

Fig.5 Five modes of the battery operation in the proposed design

Mode A: If the PV panel supplies power normally but the device in the load is turned off, the battery will absorb all the power from the input. The average charging current is positive for the battery. The proposed circuit operates with its first stage as a conventional converter. Switches can be added to disconnect the load or the second stage based on the requirement.

Mode B: When the supply power from the solar unit is greater than the load demand, the battery is charged with the excess. This mode happens when the load device operates with a light load.

Mode C: This is a situation that power supply is equal to the load demand. In this case, the battery does not absorb or supply any power. Therefore, the average of the charging current is zero.

Mode D: When the supply power is insufficient to meet the load demand due to shading or low irradiation, the battery supplies the load as a complementary power source. The battery is discharged and the average current of charging is negative in this mode.

Mode E: When there is no power provided by the PV panel, the battery will supply the load fully. This mode usually happens during the night with the insufficient irradiation. In this mode, the first stage of the proposed circuit is disabled while the second stage works as a conventional converter to supply the load. Although the diode D_1 will prevent reverse current from the battery theoretically, a protection diode can be installed for the solar unit if necessary.

3 Circuit design process

This section presents a general design process to find the parameters and the maximum ratings of the components in the proposed circuit. These values are determined by the topology of the proposed circuit as well as its operational modes which are discussed in Section 2. The calculations should be conducted with proper design requirements. The assumptions in Section II are still valid for the following analysis.

3.1 Parameters of the components

The design process starts from the second stage of the proposed circuit. Since the circuit runs in CCM in the second stage, the duty ratio D can be found easily based on the relationship of the terminal voltages V_b and V_o as follows:

$$G_2 = \frac{V_o}{V_b} = D \tag{5}$$

Note that the duty ratio D is a key factor for the whole analysis of the design process.

Based on the duty ratio D, the equivalent current I_{b2} provided by the battery can be expressed by the following equation:

$$I_{b2} = DI_o \tag{6}$$

where I_o is the output current of the load. This will be used in the analysis of the first stage as well.

Then, the inductor L_2 should be designed properly for CCM operation. The inductor value should be greater than its CCM-DCM boundary value as in the conventional design process. The inductance can be found as:

$$L_2 > \frac{(1-D)R_L}{2f} \tag{7}$$

where R_L means the resistance of the load.

The ripple of the load voltage is related to the load capacitor C_2. With the parameters of the design requirements, the size of the capacitor can be determined as:

$$\Delta V_o = \frac{1-D}{8L_2C_2f^2}V_o \tag{8}$$

Next, the components in the first stage are selected according to the parameters from the previous analysis. In a balanced case, the battery current provided by the first stage must equal to the current supplying the second stage, i.e. I_{b1}=I_{b2}. In the first stage, the equivalent resistance R_{eq} is given as follow for the convenience of calculation:

$$R_{eq} = \frac{V_b}{I_{b1}} = \frac{V_b}{I_{b2}} \tag{9}$$

Unlike the CCM mode, the DCM operation requires the inductance of L_1 remaining in the DCM zone. In other words, L_1 must be lower than its boundary value as below:

$$L_1 < \frac{D(1-D)^2 R_{eq}}{2f} \tag{10}$$

Meanwhile, the value of L_1 can be found based on the following equation of the DCM:

$$G_1 = \frac{V_b}{V_{in}} = \frac{1}{2}\left(1+\sqrt{1+\frac{2DR_{eq}}{L_1 f}}\right) \tag{11}$$

where G_1 represents the gain of the first stage. Rearranging (11) yields:

$$L_1 = \frac{2DR_{eq}T}{\left(2\frac{V_b}{V_{in}}-1\right)^2-1} \tag{12}$$

Note that in some cases, the (12) may not lead to a valid solution due to (10). In the proposed design process, it is important to maintain the power conversion in DCM in the first stage with proper parameters selections. Otherwise, the first stage can not work correctly. The characteristics of the two stages are shown in Fig.6 with the CCM-DCM boundaries when V_b is fixed due to the battery. The x-axis of the chart (a) is represented by the ratio of battery current I_{b1} to its maximum boundary current $I_{b1B,max}$. The boundary current is obtained as follows:

$$I_{b1B} = \frac{V_b}{2L_1 f}D(1-D)^2 \tag{13}$$

When D=1/3, it is equal to $I_{b1B,max}$.

Similarly, the ratio of battery current I_{b2} to its maximum boundary current $I_{b2B,max}$ is used for the x-axis of the chart (b). The boundary current is given as below:

$$I_{b2B} = \frac{V_b}{2L_2 f}D(1-D) \tag{14}$$

When D=1/2, $I_{b2B,max}$ is found.

Note that the battery current of different stages should be the equal, I_{b1}=I_{b2}, for a balanced operation. The duty ratio D should be fixed for the single switch as well. The parameters of the components can be selected based on Fig.6 to ensure the correct operational mode of each stage in the proposed design.

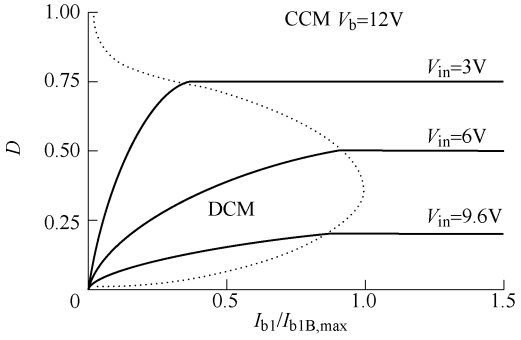

(a) The first stage

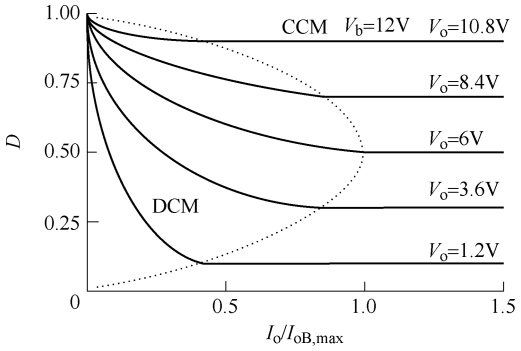

(b) The second stage

Fig.6 Converter characteristics of the two stages of the proposed design keeping the V_b constant

The capacitor C_1 absorbs the ripple component in the first stage to protect the battery. Once the parameters above are determined, the following equation gives the value of the capacitance C_1 based on the design requirements:

$$\Delta V_b = \frac{1}{2C_1}\left(\frac{D}{L_1 f}V_{in} - I_{b1}\right)\Delta_1 \tag{15}$$

Note that Δ_1 T is the interval where the proposed circuit operates in mode 2. The value of Δ_1 can be found by:

$$\frac{V_b}{V_{in}} = \frac{\Delta_1 + D}{\Delta_1} \tag{16}$$

Once the parameters of all the components are found, both stages of the proposed circuit will work with their own control variables, the frequency f and the duty ratio D, respectively. The second stage of the circuit will be regulated by the PWM controller varying D as the traditional DC-DC buck converter if CCM condition (7) is met. Meanwhile, when (10) is satisfied, the frequency f becomes a dominant variable for the first stage since the duty ratio D is relatively stable. Therefore the PFM controller governs the input with (11) in the first stage. Then the PFM+PWM control is conducted for the proposed design as the analysis above.

3.2 Maximum ratings of the components

After the sizes of the components are determined above, the maximum voltages across them should be considered wisely as well as the currents. The voltage and current stress of the proposed design are listed in Table 1 along with the data of the conventional one with independent switch control.

Table 1 Stress comparison of the proposed design with the conventional

	The proposed design		The conventional design	
Comp.	Voltage stress	Current stress	Voltage stress	Current stress
L_1		$I_{in}+\frac{V_{in}Df}{2L}$		$I_{in}+\frac{V_{in}D_1 f}{2L}$
L_2		$I_o+\frac{(V_b-V_o)Df}{2L}$		$I_o+\frac{(V_b-V_o)D_2 f}{2L}$
C_1	V_b		V_b	
C_2	V_o		V_o	
S_1	V_b	$I_{in}+\frac{V_{in}Df}{2L}+I_o+\frac{(V_b-V_o)Df}{2L}$	V_{in}	$I_{in}+\frac{V_{in}D_1 f}{2L}$
S_2	NA	NA	V_b-V_o	$I_o+\frac{(V_b-V_o)D_2 f}{2L}$
D_1	V_b	$I_{in}+\frac{V_{in}Df}{2L}$	V_b	$I_{in}+\frac{V_{in}D_1 f}{2L}$
D_2	V_b	$I_o+\frac{(V_b-V_o)Df}{2L}$	V_b	$I_o+\frac{(V_b-V_o)D_2 f}{2L}$
D_3		$I_{in}+\frac{V_{in}Df}{2L}$	NA	NA
D_4		$I_o+\frac{(V_b-V_o)Df}{2L}$	NA	NA

The expressions are used to find the minimum values of the components in steady operation. In practice, the unsteady cases should be taken into account as well as the safety margin of the stress. Some components may be facing higher voltage drops which is the V_b in those cases. In the conventional design, a MOSFET S_1 is used with the duty ratio D_1 in the first stage while S_2 with D_2 is in the second stage. D_1 and D_2 are determined by the voltages of different stages. The two switches in the conventional design are decoupled and their duty ratios are independent of each other. The empty slots in the table mean that these values are not the key factors in component selection. NA in the table indicates that the components are not used in that kind of design. The main difference between the two designs is the increased voltage and current stress in the single switch in this paper. This may not always be true when D_1 and D_2 are changed to other values.

4 Simulation and experiments

The prototype of the proposed circuit is built according to the design process in Section 5 as well as the design specifications as given in the following table:

4.1 Comparison of the key components

The main circuit of the proposed prototype is compared with the conventional design of the cascade converters. Regarding the component difference between the two designs, the proposed design has one switch less than the conventional while two more diodes are necessary to regulate the current for the single switch. The prices of these key components are summarised in Table II. The price data is provided on the website of a distributor of technology products (element14 Pty Ltd.) in Australia dollars. The prices are for prototype-making on a small scale only. However, these can reflect the advantage of the proposed design to some extent regarding the cost. The increased cost of the diodes is low compared to other components. Some cheaper components with lower ratings might be used to slightly decrease the cost in the conventional design. But in general, the proposed circuit reduces the cost of the key components by about 47%.

Moreover, the dimension of the circuit is decreased dramatically due to omitting one heat sink for the switch. The heat sink used for the switches is one of the largest components with the size of 25.4mm ×45mm ×12.7mm (L ×W ×H).

Table 2 Design specification

The first stage		The second stage		Switching	
Parameters	Value	Parameters	Value	Parameters	Value
V_{in}/V	6	V_o/V	2.4	f/kHz	15
V_b/V	12	R_L/Ω	2.5	D	0.2
L_1/μH	50	L_2/μH	100		
C_1/μF	100	C_1/μF	100		

Table 3 Cost comparison of the key components

The proposed design			
Conponents	Name	Num.	Cost/$
Switch	IRFB4110PBF MOSFET transistor	1	6.19
Switch driver	TC1427CPA	1	1.73
Diode	FR203 standard recovery diode	4	0.88
Heat sink	SK 409/25,4 STS Heat sink	1	2.26
Total			11.06
The conventional design			
Conponents	Name	Num.	Cost/$
Switch	IRFB4110PBF MOSFET transistor	2	12.38
Switch driver	TC1427CPA	2	3.46
Diode	FR203 Standard recovery diode	2	0.44
Heat sink	SK 409/25,4 STS Heat sink	2	4.52
Total			20.80

4.2 Comparison of the switching loss

One of the main power losses in the voltage conversion is the power loss in the switching. By sharing the current path, the proposed circuit is able to reduce the switching loss to some extent. With the same specification above except the fixed resistance R_L, the power loss during the on-period of the MOSFETs is compared with different input powers, P=2W and P=5W. It is assumed that the battery is in mode C which does not affect the power conversion in both stages of the proposed circuit. In both cases, V_o and V_b are fixed while V_{in} is changing for 1V to 5V. The duty ratio of the proposed design is 0.2 while the duty ratios of the conventional design are determined by the input and output voltages. IRFB4110PBF MOSFET with a very low static drain-to-source on-resistance (R_{DS}= 3.7mΩ) is used for all controlled switches in both designs. The result is shown in Fig.6. The proposed design reduces the switching loss when they are energised by up to 50%. A certain amount of loss improvement can be found in the normal operational range of V_{in}. When V_{in} is close to V_b, the performance of the proposed circuit is close to the conventional regarding the on-period switching loss.

4.3 Simulation

A simulation model is built in PSIM based on the proposed circuitry to verify the analysis in previous sections. The waveforms of the simulation are shown in Fig.8. In the simulation results, V_{con} is the control signal provided by the PWM+PFM controller with duty ratio D. The inductor current i_{L1} is a discontinuous ramp wave indicating that the first stage of the circuit works in DCM. i_{L1} drops to zero after the interval of mode 2 as expected. Meanwhile, the CCM operation of the inductor L_1 is confirmed by the continuous current

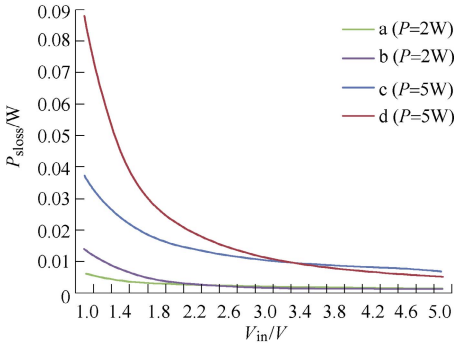

Fig.7 Comparison of the power loss of the MOSFETs in their on-period with variable V_{in}

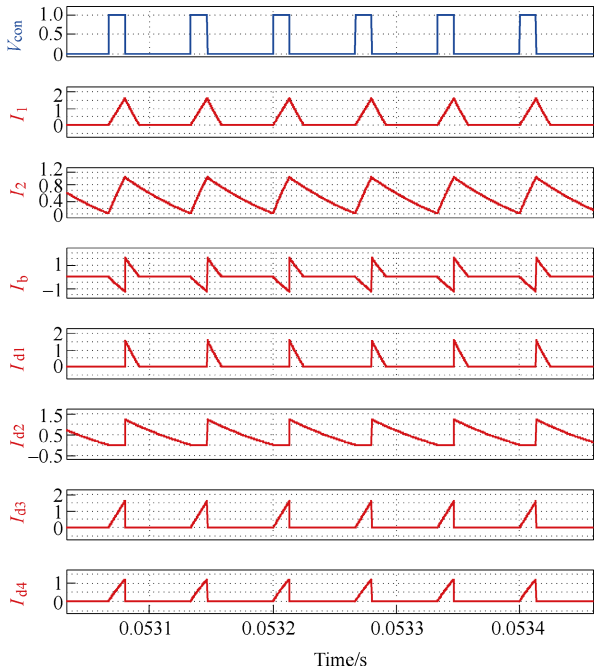

Fig.8 The simulation result of the currents flowing in different components during the switching period (V_{con}: 1V/div; i_{L1}, i_{L2}, i_b, i_{d1}~i_{d4},: 1A/div)

i_{L2} in the simulation, i.e. the current remains positive during the whole switching period. The charging current i_b of the battery is given in Fig.8. as well. The positive and negative values of i_b represent the direction of the battery current. The positive i_b indicates energy absorption when the single switch is energised. By contrast, the negative means the battery is discharging and supplying the second stage. The diode current i_{d1}~i_{d4} from the simulation verify the operation of the proposed circuit in detail. Diode D_1 and D_2 function similarly to the conventional converters while the D_3 and D_4 help the single switch to work properly.

The voltage of the two ends of the proposed circuit, V_{in} and V_o, are found in the simulation as well as the ramp signal V_{ramp} as shown in Fig.9. Both voltages satisfied the design specification in the previous sections.

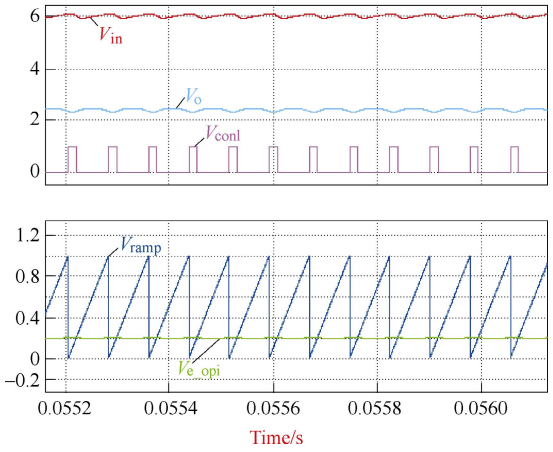

Fig.9 Simulation results of voltages and the ramp signal in the proposed design (V_{in}, V_o, V_{con}: 2V/div; V_{ramp}, $V_{e\_o\_pi}$: 0.2V/div)

4.4 Experimental results

The prototype tested in this study has the same specification as the previous simulation. It connects the PV power source with the storage unit and the load as the circuit diagrams in the previous analysis. Similar to the simulation model, the prototype ensures the steady output voltage as well as the input. The waveforms of the inductor currents observed from an oscilloscope confirm the DCM operation of the inductor L_1 along with the CCM mode of the inductor L_2, as shown in Fig.10(a). Moreover, the battery works like the analysis because the waveform of its current i_b is the same as the simulation result. The experimental results verify the correct operation of the proposed design.

The efficiency of the proposed design is compared with the conventional one in different shading conditions of the PV panel in Fig.11. The efficiency is improved by about 4% by the proposed design.

5 Conclusion

A design of two-stage DC-DC converters with a single switch is introduced in this paper for off-grid solar power applications. The main switches of the conventional design are substituted by one single switch with some auxiliary diodes. The proposed design is described with its main circuit as well as its control schemes. With the help of PFM+PWM modulation, the proposed circuit is able to function as the conventional design with the single switch. Furthermore, the size, the cost and the power loss are improved by the new design in this paper. The design process is provided with the analysis of the proposed circuit. The waveforms of the simulation and experimental results validate the function of the proposed

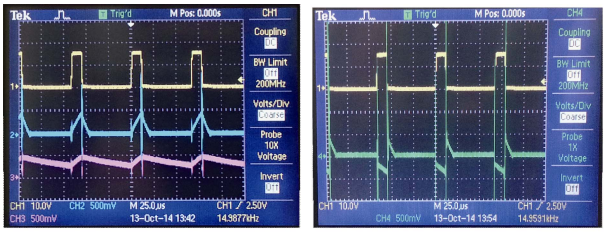

(a) CH1: V_{con}; CH2: i_{L1}; CH3: i_{L2} (b) CH1: V_{con}; CH2: i_b.

Fig.10 The experimental results

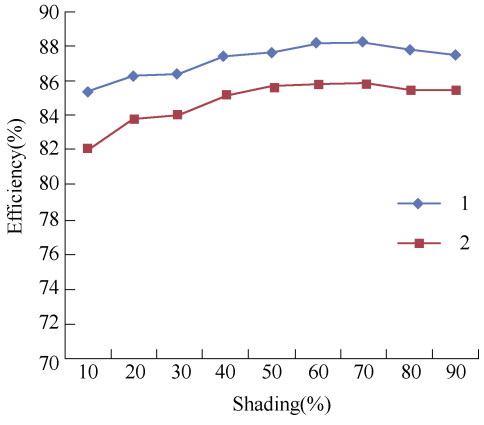

Fig.11 The efficiency comparison of different shading conditions: η_1: The proposed design; η_2: The conventional design

circuit. This circuit is well suited for the application of standalone power systems and provides better performance than the conventional design.

The proposed study has a broad range of perspectives and can be investigated further for several issues. The application in other renewable power systems could be studied as well as on-grid power systems. Moreover, the auxiliary and protection circuits can be developed for low irradiation situation and the extreme cases of the battery (exhausted or full-charge SOC). The rearrangement of the regulation schemes can be discussed in the future as well.

Acknowledgment

The authors are grateful to Prof. D. D. C. Lu and Dr. L. An for improving the quality of the paper.

References

[1] P. S. Shenoy, K. A. Kim, B. B. Johnson, and P. T. Krein, "Differential power processing for increased energy production and reliability of photovoltaic systems," *IEEE Transactions on Power Electronics*, vol. 28, no. 6, pp. 2968-2979, 2013.

[2] X. Lu, K. Sun, J. M. Guerrero, J. C. Vasquez, and L. Huang, "State-of-charge balance using adaptive droop control for distributed energy storage systems in DC microgrid applications," *IEEE Transactions on Industrial Electronics*, vol. 61, no. 6, pp. 2804-2815, 2014.

[3] G. R. Walker, and P. C. Sernia, "Cascaded DC-DC converter connection of photovoltaic modules," *IEEE Transactions on Power Electronics*, vol. 19, no. 4, pp. 1130-1139, 2004.

[4] X. Xiong, C. K. Tse, and X. Ruan, "Bifurcation analysis and experimental study of a multi-operating-mode photovoltaic-battery hybrid power system," *IEEE Journal on Emerging and Selected Topics in Circuits and Systems*, vol. 5, no. 3, pp. 316-325, 2015.

[5] W. Li, and X. He, "Review of nonisolated high-step-up DC/DC converters in photovoltaic grid-connected applications," *IEEE Transactions on Industrial Electronics*, vol. 58, no. 4, pp. 1239-1250, 2011.

[6] M. Forouzesh, K. Yari, A. Baghramian, and S. Hasanpour, "Single-switch high step-up converter based on coupled inductor and switched capacitor techniques with quasi-resonant operation," *IET Power Electronics*, vol. 10, no. 2, pp. 240-250, 2017.

[7] H. Wang, Y. Chen, Y. F. Liu, J. Afsharian, and Z. Yang, "A passive current sharing method with common inductor multiphase LLC resonant converter," *IEEE Transactions on Power Electronics*, vol. 32, no. 32, pp. 6994-7010, 2017.

[8] Y. K. Ramadass,and A. P. Chandrakasan, "An efficient piezoelectric energy harvesting interface circuit using a bias-flip rectifier and shared inductor," *IEEE Journal of Solid-State Circuits*, vol. 45, no. 1, pp. 189-204, 2010.

[9] L. An, and D. D. C. Lu, "Design of a single-switch DC/DC converter for a PV-battery-powered pump system with PFM+PWM control," *IEEE Transactions on Industrial Electronics*, vol. 62, no. 2, pp. 910-921, 2015.

[10] K. H. Lee, E. Chung, Y. Han, and J. I. Ha, "A family of high-frequency single-switch DC-DC converters with low switch voltage stress based on impedance networks," *IEEE Transactions on Power Electronics*, vol. 32, no. 4, pp. 2913-2924, 2017.

[11] K. C. Tseng, C. C. Huang, and C. A. Cheng, "A single-switch converter with high step-up gain and low diode voltage stress suitable for green power-source conversion," *IEEE Journal of Emerging and Selected Topics in Power Electronics*, vol. 4, no. 2, pp. 363-372, 2016.

[12] J. J. Lee, J. M. Kwon, E. H. Kim, W. Y. Choi, and B. H. Kwon, "Single-stage single-switch PFC flyback converter using a synchronous rectifier," *IEEE Transactions on Industrial Electronics*, vol. 55, no. 3, pp. 1352-1365, 2008.

[13] S. Sharifi, M. Jabbari, and H. Farzanehfard, "A new family of single-switch ZVS resonant converters," *IEEE Transactions on Industrial Electronics*, vol. 64, no. 6, pp. 4539-4548, 2017.

[14] H. H. Wu, C. L. Wei, Y. C. Hsu, and R. B. Darling, "Adaptive peak-inductor-current-controlled PFM boost converter with a near-threshold startup voltage and high efficiency," *IEEE Transactions on Power Electronics*, vol. 30, no. 4, pp. 1956-1965, 2015.

Junkai Zhao (S'15) obtained his B.Eng. degree in integrated circuits design and integrated systems from Xidian University, China, in 2010 and Master's degree in electrical and electronic engineering with distinction from the University of Western Australia in 2013. He is currently pursuing his Ph.D. degree at the University of Western Australia.

His research interests are in power electronics, power conversion and renewable energy.

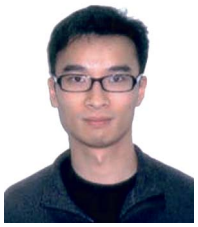

Herbert Ho-Ching Iu (S'98–M'00–SM'06) received the B.Eng. (Hons) degree in electrical and electronic engineering from the University of Hong Kong, Hong Kong, in 1997. He received the Ph.D. degree from the Hong Kong Polytechnic University, Hong Kong, in 2000.

In 2002, he joined the School of Electrical, Electronic and Computer Engineering, The University of Western Australia where he is currently a Professor. His research interests include power electronics, renewable energy, nonlinear dynamics, current sensing techniques, and memristive systems.

Prof. Iu currently serves as a Guest Editor for the IEEE Transactions on Industrial Electronics and several other journals including IET Power Electronics.

Tyrone Fernando (M'95–SM'05) obtained his bachelor of engineering with honours and the degree of doctor of philosophy from the University of Melbourne in 1990 and 1996 respectively.

In 1996 he joined the University of Western Australia, School of Electrical Electronic and Computer Engineering where he is currently a Professor. His research interests are in functional observers, state estimation, control theory and power systems and biomedical engineering.

Prof. Fernando has served as an Associate Editor for the IEEE Transactions on Information Technology in Biomedicine and also as guest editor for the Journal of Optimal Control Applications and Methods. He is currently an associate editor for the IEEE Transactions on Circuits and Systems II.